Carbon dioxide ice clouds, snowfalls, and baroclinic waves in the northern winter polar atmosphere of Mars

Takeshi Kuroda,[1] Alexander S. Medvedev,[2] Yasumasa Kasaba,[1] and Paul Hartogh[2]

Received 14 December 2012; revised 27 February 2013; accepted 6 March 2013; published 28 April 2013.

[1] The formation of CO_2 ice clouds in the northern winter polar atmosphere of Mars and their relation to baroclinic planetary waves, which dominate local dynamics, are studied using a general circulation model. The simulation shows that clouds are formed at altitudes of up to ∼40 km, and their occurrence correlates to a large degree with the cold phases of transient planetary waves. Ice particles formed up to ∼20 km can reach the surface in the form of snowfall in certain longitude regions, while in others, these particles likely sublimate in the lower warmer atmospheric layers. The simulation suggests that about a half of the seasonal ice cap is created by CO_2 snow, while the remaining half by direct condensation on the surface. Thus, the occurrences of ice clouds and rates of deposition are closely linked to traveling planetary waves, indicating the possibility for the reliable forecasts of CO_2 snow storms.
Citation: Kuroda, T., A. S. Medvedev, Y. Kasaba, and P. Hartogh (2013), Carbon dioxide ice clouds, snowfalls, and baroclinic waves in the northern winter polar atmosphere of Mars, *Geophys. Res. Lett.*, *40*, 1484–1488, doi:10.1002/grl.50326.

1. Introduction

[2] The martian atmosphere is mainly (95.3%) composed of CO_2. When the temperature drops below the CO_2 condensation level (∼145 K at 6 hPa), mainly in the winter polar regions, the CO_2 condenses to form ice. This process significantly changes the total mass of the martian atmosphere. Measurements from Viking landers showed annual variations of 25% in the surface pressure, with the maximum pressure being observed around the northern winter solstices, and the minimum in the northern summers [*Tillman et al.*, 1993].

[3] The seasonal polar caps are formed from condensed CO_2. The northern polar cap extends to ∼60°N at the spring equinox, recesses almost linearly during the spring, and disappears at the summer solstice, leaving only the residual cap that consists of water ice [*Cantor et al.*, 1998; *Iwasaki et al.*, 1999; *James and Cantor*, 2001]. Observations using the Thermal Emission Spectrometer (TES) [*Kieffer and Titus*, 2001] and the Mars Orbiter Laser Altimeter (MOLA) [*Smith et al.*, 2001], onboard the Mars Global Surveyor (MGS) spacecraft, indicate that the accumulated CO_2 ice in snow at the seasonal northern cap is up to 1.5 m deep.

[4] The seasonal CO_2 polar cap appears to be formed from ice particles that have fallen from the atmosphere as well as those condensed directly on the surface. Using brightness temperature measurements from Mariner 9 and the Viking spacecraft [*Kieffer et al.*, 1976, 1977], *Forget et al.* [1995] pointed to the possible occurrence of CO_2 snowfall in the winter polar regions. MGS-MOLA observed cloud echoes below ∼20 km during polar winters [*Colaprete et al.*, 2003]. *Colaprete et al.* [2008] found temperatures causing supersaturation of CO_2 gas in the MGS-TES observations, and simulated CO_2 snowfall using a martian general circulation model (MGCM), which revealed longitudinal irregularities of CO_2 ice clouds in the northern polar region thought to be linked to local weather phenomena ("storm zones") [*Hollingsworth et al.*, 1996]. Our study addresses the mechanism by which atmospheric dynamics affect the occurrence of CO_2 ice clouds and snowfalls in high latitudes during northern winter.

[5] Transient planetary waves are a prominent feature of martian atmospheric dynamics during northern winters, and were first detected in the time series of surface pressure taken by the Viking Landers [*Barnes*, 1980, 1981]. The waves were investigated in more detail using the MGS-TES [*Wilson et al.*, 2002; *Banfield et al.*, 2004] and then with radio occultation data [*Hinson*, 2006] as well as with MGCMs [*Barnes et al.*, 1993; *Collins et al.*, 1996; *Wilson et al.*, 2002; *Kuroda et al.*, 2007]. From northern autumn to spring, eastward traveling waves with a zonal wave number of $s = 1$ and periods of 5–6 sols (solar days on Mars) or longer exist in northern mid-latitudes. Components with $s = 2$ and $s = 3$, which have correspondingly shorter periods, are also present near the surface. *Wilson et al.* [2002] and *Banfield et al.* [2004] showed that the latter waves are generated by a baroclinic instability in the lower atmosphere, while barotropic processes contribute to the former, approximately above the first scale height. *Kuroda et al.* [2007] demonstrated that the $s = 1$ and $s = 2$ harmonics have comparable amplitudes before the winter solstice, while the $s = 1$ waves dominate afterward. The amplitude of transient waves is much smaller during southern hemisphere winters [*Banfield et al.*, 2004].

[6] In this work, we use our MGCM with an implemented simple scheme representing the formation and transport of CO_2 ice clouds to investigate snowfall in high latitudes during northern winters. Emphasis is put on the dynamical influence of transient planetary waves. The MGCM and CO_2 cloud scheme are outlined in section 2. Results of the simulations for the northern winter season are presented in section 3. Discussion and conclusions are given in section 4.

[1]Department of Geophysics, Tohoku University, Sendai, Japan.
[2]Max Planck Institute for Solar System Research, Katlenburg-Lindau, Germany.

Corresponding author: T. Kuroda, Planetary Plasma and Atmospheric Research Center, Tohoku University, Sendai, Japan. (tkuroda@pat.gp.tohoku.ac.jp)

0094-8276/13/10.1002/grl.50326

2. Outline of the MGCM

[7] The MGCM used in this study is based on a terrestrial GCM developed collaboratively between the Center for Climate System Research, University of Tokyo, National Institute of Environmental Studies, and the Frontier Research Center for Global Change (CCSR/NIES/FRCGC) in Japan [*K-1 Model Developers*, 2004]. It utilizes a spectral solver for the three-dimensional primitive equations, and has a set of physical parameterizations for the martian atmosphere as described in *Kuroda et al.* [2005], which account in particular for the radiative effects of gaseous CO_2 and airborne dust. The model has been validated against the observed zonal mean climatology [*Kuroda et al.*, 2005], and has been applied to the study of baroclinic planetary waves [*Kuroda et al.,* 2007],zonal-mean variability in mid-andhigh-latitudes [*Yamashita et al.*, 2007], equatorial semiannual oscillations [*Kuroda et al.*, 2008], and winter polar warmings during global dust storms [*Kuroda et al.*, 2009].

[8] In this study, a modified version of CO_2 condensation/sublimation scheme from *Kuroda et al.* [2005], in which the condensed CO_2 ice was allowed to fall on the surface instantaneously, has been used. The modified version accounts for the finite velocity of gravitational sedimentation, and considers the horizontal and vertical transport of CO_2 ice clouds. If our model predicts a temperature drop below the carbon dioxide supersaturation level, an ice cloud forms, and latent heat is released to maintain the degree of supersaturation. The CO_2 saturation temperature T_s is calculated as the function of pressure p with the Clausius-Clapeyron relation for perfect gas [*Hourdin et al.*, 1995]:

$$T_s = \left(\frac{1}{T_0} - \frac{R \ln(p/p_0)}{L} \right)^{-1}, \tag{1}$$

where R is the gas constant; T_0 = 136.3 K is the reference saturation temperature at p_0 = 1 hPa; and $L = 5.9 \times 10^5$ J kg^{-1} is the latent heat of CO_2. The significant degree of supersaturation required to heterogeneously nucleate CO_2 cloud particles is accounted for by using $1.35 \times p$ instead of pressure, as suggested by *Glandorf et al.* [2002]. This definition of supersaturation agrees well with the observations of lower polar atmosphere during winter by MGS-TES [*Colaprete et al.,*2008] and radio occultation [*Hu et al.*, 2012]. The sedimentation velocity for CO_2 ice particles w is calculated from Stokes' law with the modifications of *Kasten* [1968]:

$$w = \frac{2\rho_d g r^2}{9\eta} F, \tag{2}$$

where $F = 1 + (\lambda/r)(A + B\exp\{-Cr/\lambda\})$ is the factor defined by *Kasten* [1968] with dimensionless empirical constants A, B, C, mean free path length λ; ρ_d = 1600 kg m^{-3} is the density of CO_2 ice; g is the acceleration of gravity; η is the dynamic viscosity. The radius of cloud particles r is defined as a function of height z:

$$r(z) = r_0 \exp(-z/h), \tag{3}$$

where r_0 is the particle radius at z = 0 km, and h is the corresponding scale height. *Forget et al.* [1995] estimated that radii of CO_2 ice particles, which exist during polar nights below ∼20 km, are between 10 and 50 μm. Recently observed mesospheric CO_2 ice particles are estimated to have radii of between 1 and 2 μm at ∼80 km [*Montmessin et al.*, 2007], and ∼0.1 μm at ∼100 km [*Montmessin et al.*, 2006]. The distribution (3) with r_0 = 50 μm and h = 20 km approximately satisfies the above observational constrains.

[9] In our simulations, the horizontal resolution of the model was set to T21 (about 5.6° × 5.6°, ∼333 km at the equator), and the vertical grid consisted of 69 σ-levels with the top of the model set at about 100 km. Local thermodynamic equilibrium (LTE) was assumed for radiative calculations at all heights. We employed seasonal and latitudinal distributions of the dust opacity for Mars Year 29 [e.g., *Smith*, 2009], and accounted for the surface roughness as derived by *Heavens et al.* [2008].

3. Results

[10] Figure 1 compares the observed and simulated zonal mean temperature and aerosol mass mixing ratios in the northern hemisphere averaged over the winter season between L_s = 255° and 285° during relatively low-dust conditions. Observations represent the MRO-MCS Derived Data Version 2 [*Kleinböhl et al.*, 2009] for MY29, which is publicly available at the NASA Planetary Data System. As *McCleese et al.* [2010] argue, the dust signals in retrievals in winter polar regions are likely to be caused by CO_2 ice clouds. Following *McCleese et al.* [2010], we consider such dust signals as the evidence for CO_2 ice clouds. The mass mixing ratio of particles (either dust, or CO_2 ice) q_d was calculated from the retrieved opacities per height $\Delta\tau/\Delta z$:

$$q_d = \frac{\Delta\tau}{\Delta z} \frac{4}{3} \frac{r_{\text{eff}}\, \rho_d}{Q_e\, \rho}. \tag{4}$$

In (4), r_{eff} and Q_e are the effective radius, and the extinction efficiency of particles, respectively; ρ is the atmospheric density. We used r_{eff} = 1.5 μm following the definition of dust properties in the retrieval calculations of opacities [*Kleinböhl et al.*, 2009]. Q_e is set to 0.0027, based on the properties of CO_2 ice clouds [*Hayne et al.*, 2012].

[11] Figure 1a demonstrates the presence of atmospheric ice particles northward of 70°N between 10 and 100 Pa (15–40 km). Simulations of temperature and mass mixing ratios of CO_2 snow, shown in Figure 1b, are in good agreement with the observations, at least in the case of the zonal mean values. In addition to the ice clouds in the polar night region, the model also simulates mesospheric CO_2 clouds in mid-latitudes, which are consistent with the Thermal Emission Imaging System (THEMIS) measurements onboard Mars Odyssey [*McConnochie et al.*, 2010]. Note that the MRO-MCS does not observe these particles (Figure 1a), because its detections are limited to altitudes below ∼10 Pa [*McCleese et al.*, 2010].

[12] We now turn to the temporal and zonal variations in the fields simulated with the MGCM. Figure 2a presents the Hovmöller diagram for the temperature and mixing ratio of CO_2 ice mass at 80°N and at a 50 Pa pressure level (∼25 km). The time range covers 95 winter sols between L_s = 255° and 315°. The running averages over one sol were applied to the plotted quantities to eliminate shorter-period variability unrelated to planetary waves. The temperature field demonstrates eastward propagating disturbances associated with traveling waves throughout the winter season. The dominant wave is s = 1 (5–6 sols period), particularly

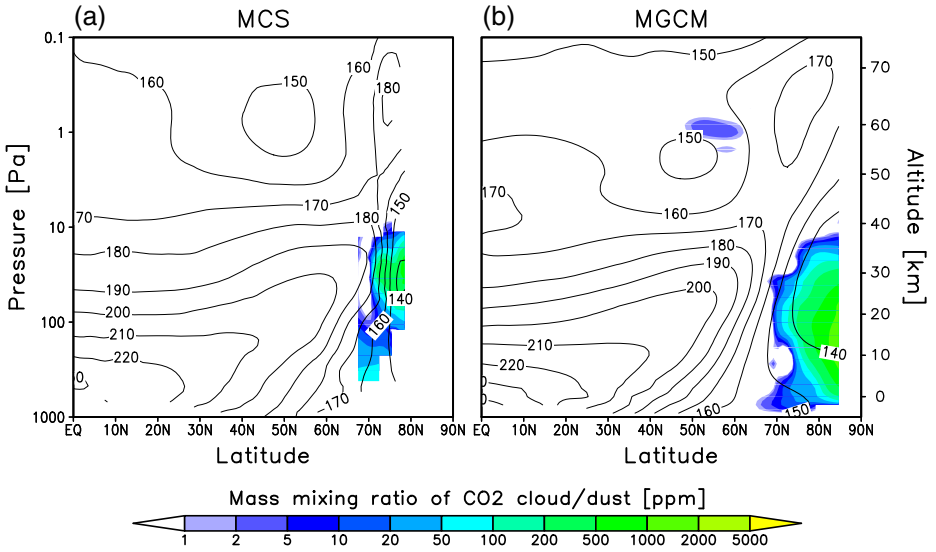

Figure 1. (a) MRO-MCS observations of the zonal mean temperature (contours) and dust (snow) mass mixing ratio (color-shaded, only north of 65°N) averaged between L_s = 255° and 285° of MY29. (b) Same as in Figure 1a, except for the simulation with the MGCM. Shades of color represent the mass mixing ratio of CO_2 ice.

after the solstice, while the component s = 2 is more significant before. As shown by *Kuroda et al.* [2007], this is due to the change in the meridional temperature gradient affecting the baroclinic instability that maintains the transient waves.

[13] From Figure 2a, it is apparent that the occurrence of CO_2 ice clouds is very much aligned with cold phases of the baroclinic waves. Although the amplitudes of wave-induced variations in temperature are of the order of a few degrees Kelvin, they are sufficient enough to modulate the CO_2 cloud formation by dropping the local air temperature below the condensation threshold. Wave-induced transport also affects the ice clouds. This shows that their behavior is complex and they do not simply follow temperature minima

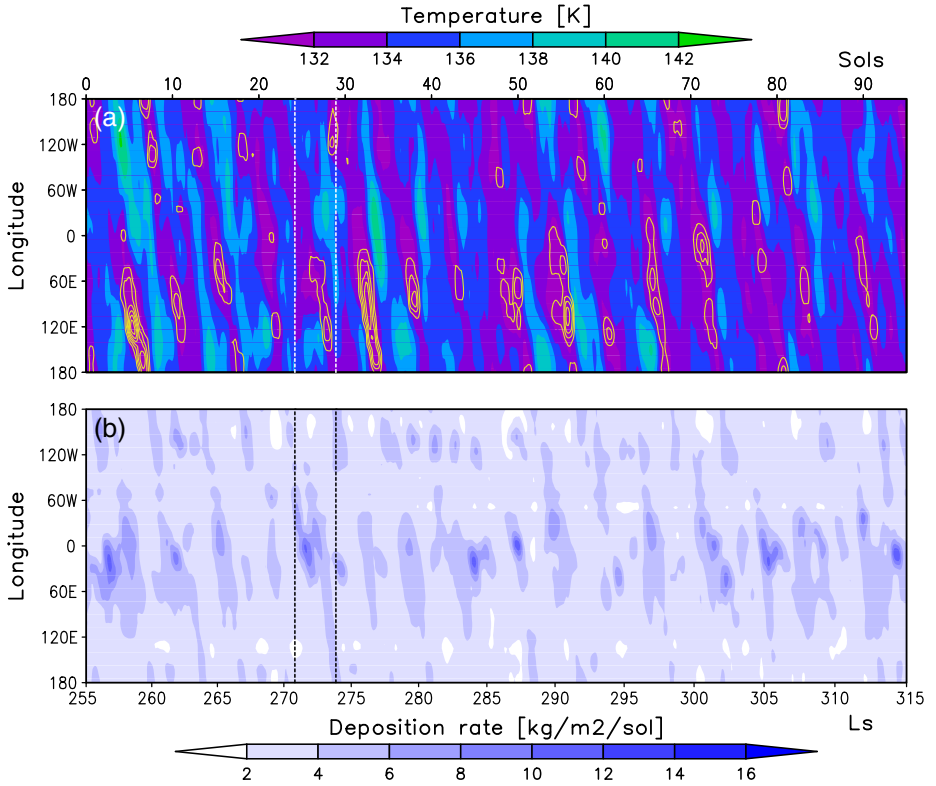

Figure 2. (a) Hovmöller diagrams of daily-averaged temperature (color shaded) and mass mixing ratios of CO_2 ice clouds (contour interval is 2000 ppm) at 80°N and 50 Pa. The dotted lines represent L_s = 270.7° and 273.9°, which correspond to the times presented in Figures 3a and 3f, respectively. (b) Same as in Figure 2a, except for the deposition rate on the surface (in kg m^{-2} sol^{-1}).

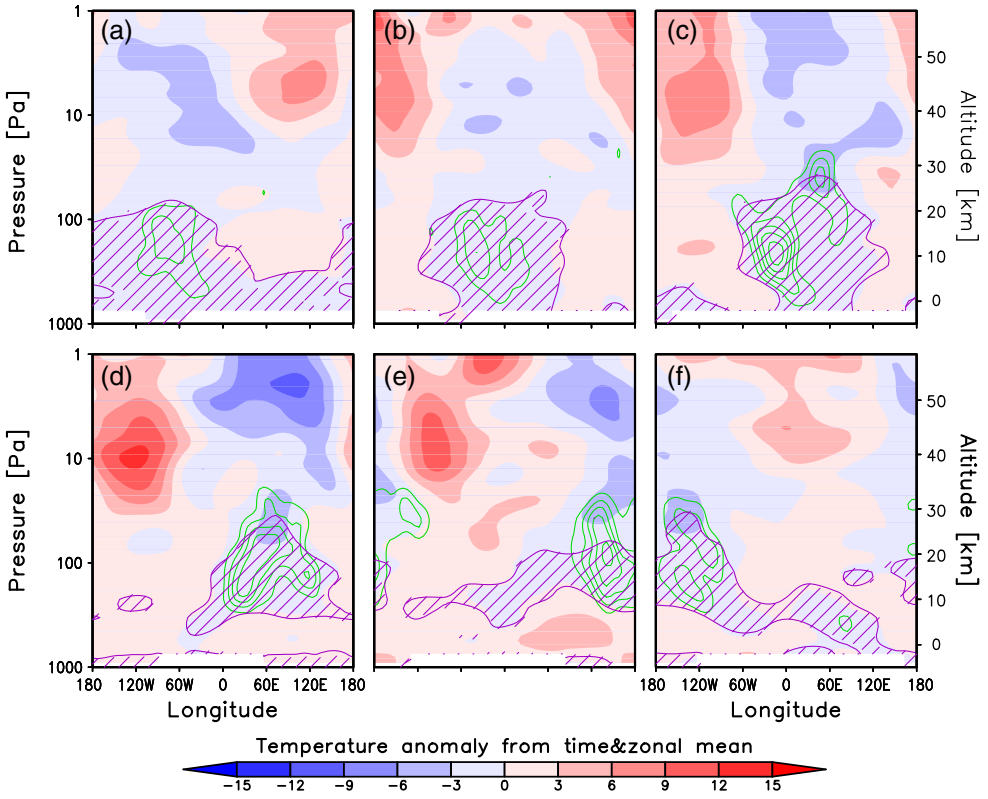

Figure 3. Longitude-height cross-sections of the simulated daily-averaged temperature and CO_2 ice clouds at 80°N: (a–f) represent the L_s = 270.7°, 271.3°, 271.9°, 272.6°, 273.2° and 273.9°, respectively (1 sol interval). Shades of color show the deviation of temperature from the zonal- and time-mean values for the shown period. Contours show the mass mixing ratio of CO_2 ice clouds (intervals of 1000 ppm). Hatched areas show regions where temperature is below the saturation level.

in the waves. It can also be noticed that the clouds occur more often around 60°E–120°E and 90°N–120°W before $L_s \sim 275°$. From this, and until $L_s \sim 290°$, they appear mostly between 60°E and 150°E. This is consistent with the above-mentioned seasonal change of the amplitudes of harmonics $s = 1$ and $s = 2$.

[14] The time-longitude cross section of the CO_2 ice deposition rate on the surface at the same latitude (80°N) is plotted in Figure 2b. Calculations show that about 58% of the ice is created by direct condensation, and the rest is due to snowfalls. The sensitivity of this ratio to the abundance of ice nuclei in the atmosphere is small. The calculations with different degrees of supersaturation (S = 1 to 2) showed less than 2% difference in the partition ratio. It is clear that the deposition rate is also modulated by transient planetary waves. In the lower atmosphere, harmonics with $s = 2$ and shorter periods dominate the $s = 1$ (5–6 sols), especially before the winter solstice [*Kuroda et al.*, 2007], which also projects on the deposition rates. In addition, the simulations demonstrate a systematic latitudinal bias in the deposition rates with more CO_2 snow reaching the surface between 30°W and 60°E.

[15] However, in our simulation, the wave-modulated time-longitude distributions of CO_2 clouds at 50 Pa (Figure 2a) do not match the deposition rates on the surface (Figure 2b). What is the relationship between the CO_2 ice clouds in the upper layers and the ice cap on the ground? Figure 3 presents the time sequence (with a 1 sol interval) of vertical distributions of daily-averaged CO_2 ice abundance for the time period, marked by two dotted lines in Figure 2. A clear wave-induced variation of temperature (color-shaded) with $s = 1$ (5–6 sols) is seen at ~300 Pa (~10 km height) and higher. Traveling waves at these heights have a barotropic structure, and show almost no vertical phase tilt.

[16] The deposition rate on the surface below, however, is not proportionally large. As shown in (2), it takes ~0.2 sols for particles to descend from 25 km to the surface, which is much shorter than the periods of the transient waves. Thus, the fate of ice particles during sedimentation depends on the thermal structure below. Areas where airborne ice can exist are shown in Figure 3 (hatched areas). Regions where the warmer and colder anomalies vertically alternate can be seen in Figures 3d–3f, where much of the falling snow sublimates in the lower layers. At 30°W–60°E, where the deposition rate is at its largest, temperatures between the surface and 10–20 km stay below the condensation point and favor falling the higher-altitude ice particles to the surface (Figures 3a–3c).

4. Conclusions

[17] We explored the formation and behavior of CO_2 ice clouds in the northern winter polar atmosphere of Mars using a general circulation model with an updated CO_2 condensation/sublimation scheme. The main results of this investigation are summarized below.

[18] Calculations show that CO_2 ice clouds are created at altitudes of up to 40 km and northward of ~70°N during northern winters. Their distribution is consistent with the MRO-MCS retrieval, at least in terms of zonally averaged

quantities. The occurrence of ice clouds is very much aligned with the cold phases of eastward propagating planetary waves, which are the dominant features of the high-latitude atmospheric dynamics in northern winters. Seasonal and vertical variations in these waves strongly project on cloud distribution.

[19] CO_2 ice particles formed below ∼20 km reach the surface, especially between 30°W and 60°E (at 80°N), where the maximum of the deposition occurs. In other longitudes, the phases of the transient waves change in the course of their descent, and the ice particles are likely to sublimate when they encounter wave-modulated temperatures above saturation values.

[20] Deposition rates on the surface are strongly modulated by transient planetary waves. Given the regular nature of such waves, this suggests that statistics of the occurrence of such snow events in high latitudes may be reliably predicted.

[21] To date, the number of observations by MRO-MCS in northern polar latitudes during winter is not enough to detect longitudinal variations of CO_2 ice clouds (see Table 3 in *Hu et al.* [2012]). More measurements concerning the temporal and longitudinal distributions of clouds, their link to planetary waves and their possible role in the formation of the seasonal ice caps, may help to validate the predictions of this study.

[22] **Acknowledgments.** This work was partially supported by the Japan Society for the Promotion of Science (JSPS) KAKENHI Grant Numbers 20-1761, 24740317; and Tohoku University Global COE Program "Global Education and Research Center for Earth and Planetary Dynamics". Comments of the anonymous reviewer helped to improve the presentation.

References

Banfield, D., B. J. Conrath, P. J. Gierasch, R. J. Wilson, and M. D. Smith (2004), Traveling waves in the martian atmosphere from MGS TES nadir data, *Icarus*, *170*, 365–403.

Barnes, J. R. (1980), Time spectral analysis of midlatitude disturbances in the Martian atmosphere, *J. Atmos. Sci.*, *37*, 2002–2015.

Barnes, J. R. (1981), Midlatitude disturbances in the Martian atmosphere: A second Mars year, *J. Atmos. Sci.*, *37*, 225–234.

Barnes, J. R., J. B. Pollack, R. M. Haberle, C. B. Leovy, R. W. Zurek, H. Lee, and J. Schaeffer (1993), Mars atmospheric dynamics as simulated by the NASA Ames general circulation model 2. Transient baroclinic eddies, *J. Geophys. Res.*, *98*, 3125–3148.

Collins, M., S. R. Lewis, P. L. Read, and F. Hourdin (1996), Baroclinic wave transitions in the Martian atmosphere, *Icarus*, *120*, 344–357.

Cantor, B. A., M. J. Wolff, P. B. James, and E. Higgs (1998), Regression of Martian north polar cap: 1990–1997 Hubble space telescope observations, *Icarus*, *136*, 175–191.

Colaprete, A., R. M. Haberle, and O. B. Toon (2003), Formation of convective carbon dioxide clouds near the south pole of Mars, *J. Geophys. Res.*, *108*, 5081, doi:10.1029/2003JE002053.

Colaprete, A., J. R. Barnes, R. M. Haberle, and F. Montmessin (2008), CO_2 clouds, CAPE and convection on Mars: Observations and general circulation modeling, *Planet. Spa. Sci.*, *56*, 150–180.

Forget, F., G. B. Hansen, and J. B. Pollack (1995), Low brightness temperatures of Martian polar caps: CO_2 clouds or low surface emissivity? *J. Geophys. Res.*, *100*, 21219–21234.

Glandorf, D. L., A. Colaprete, M. A. Tolbert, and O. B. Toon (2002), CO_2 snow on Mars and early Earth: Experimental constraints, *Icarus*, *160*, 66–72.

Hayne, P. O., D. A. Paige, J. T. Schofield, D. M. Kass, A. Kleinböhl, N. G. Heavens, and D. J. McCleese (2012), Carbon dioxide snow clouds on Mars: South polar winter observations by the Mars Climate Sounder, *J. Geophys. Res.*, *117*, E08014, doi:10.1029/2011JE004040.

Heavens, N. G., M. I. Richardson, and A. D. Toigo (2008), Two aerodynamic roughness maps derived from Mars Orbiter Laser Altimeter (MOLA) data and their effects on boundary layer properties in a Mars general circulation model (GCM), *J. Geophys. Res.*, *113*, E02014, doi:10.1029/2007JE002991.

Hinson, D. P. (2006), Radio occultation measurements of transient eddies in the northern hemisphere of Mars, *J. Geophys. Res.*, *111*, E05002, doi:10.1029/2005JE002612.

Hollingsworth, J. L., R. M. Haberle, J. R. Barnes, A. F. C. Bridger, J. B. Pollack, H. Lee, and J. Schaeffer (1996), Orographic control of storm zones on Mars, *Nature*, *380*, 413–416.

Hourdin, F., F. Forget, and O. Talagrand (1995), The sensitivity of the Martian surface pressure and atmospheric mass budget to various parameters: A comparison between numerical simulations and Viking observations, *J. Geophys. Res.*, *100*, 5501–5523.

Hu, R., K. Cahoy, and M. T. Zuber (2012), Mars atmospheric CO_2 condensation above the north and south poles as revealed by radio occultation, climate sounder, and laser ranging observations, *J. Geophys. Res.*, *117*, E07002, doi:10.1029/2012JE004087.

Iwasaki, K., D. C. Parker, S. Larson, and T. Akabane (1999), Martian north polar cap 1996–1997, *Icarus*, *138*, 20–24.

James, P. B., and B. A. Cantor (2001), Martian north polar cap recession: 2000 Mars orbiter camera observations, *Icarus*, *154*, 131–144.

K-1 Model Developers, (2004), K-1 coupled GCM (MIROC) description, *K-1 Tech. Rep. 1*, pp. 1–34, Univ. of Tokyo, Tokyo.

Kasten, F. (1968), Falling speed of aerosol particles, *J. Appl. Meteor.*, *7*, 944–947.

Kieffer, H. H., S. C. Chase, E. D. Miner, F. D. Palluconi, G. Münch, G. Neugebauer, and T. Z. Martin (1976), Infrared thermal mapping of the Martian surface and atmosphere: First results, *Science*, *198*, 780–786.

Kieffer, H. H., T. Z. Martin, R. Peterfreund, B. M. Jakosky, E. D. Miner, and F. D. Palluconi (1977), Thermal and albedo mapping of Mars during the Viking primary mission, *J. Geophys. Res.*, *82*, 4249–4291.

Kieffer, H. H., and T. N. Titus (2001), TES mapping of Mars' North seasonal cap, *Icarus*, *154*, 162–180.

Kleinböhl, A., et al. (2009), Mars Climate Sounder limb profile retrieval of atmospheric temperature, pressure, and dust and water ice opacity, *J. Geophys. Res.*, *114*, E10006, doi:10.1029/2009JE003358.

Kuroda, T., N. Hashimoto, D. Sakai, and M. Takahashi (2005), Simulation of the Martian atmosphere using a CCSR/NIES AGCM, *J. Meteor. Soc. Japan*, *83*, 1–19.

Kuroda, T., A. S. Medvedev, P. Hartogh, and M. Takahashi (2007), Seasonal changes of the baroclinic wave activity in the northern hemisphere of Mars simulated with a GCM, *Geophys. Res. Lett.*, *34*, L09203, doi:10.1029/2006GL028816.

Kuroda, T., A. S. Medvedev, P. Hartogh, and M. Takahashi (2008), Semiannual oscillations in the atmosphere of Mars, *Geophys. Res. Lett.*, *34*, L23202, doi:10.1029/2008GL036061.

Kuroda, T., A. S. Medvedev, P. Hartogh, and M. Takahashi (2009), On forcing the winter polar warmings in the Martian middle atmosphere during dust storms, *J. Meteor. Soc. Japan*, *87*, 913–921.

McCleese, D. J., et al. (2010), Structure and dynamics of the Martian lower and middle atmosphere as observed by the Mars Climate Sounder: Seasonal variations in zonal mean temperature, dust, and water ice aerosols, *J. Geophys. Res.*, *115*, E12016, doi:10.1029/2010JE003677.

McConnochie, T. H., J. F. Bell III, D. Savransky, M. J. Wolff, A. D. Toigo, H. Wang, M. I. Richardson, and P. R. Christensen (2010), THEMIS-VIS observations of clouds in the martian mesosphere: Altitudes, wind speeds, and decameter-scale morphology, *Icarus*, *210*, 545–565.

Montmessin, F., E. Quémerais, J. L. Bertaux, O. Korablev, P. Rannou, and S. Lebonnois (2006), Stellar occultations at UV wavelengths by the SPICAM instrument: Retrieval and analysis of Martian haze profiles, *J. Geophys. Res.*, *111*, E09S09, doi:10.1029/2005JE002662.

Montmessin, F., B. Gondet, J.-P. Bibring, Y. Langevin, P. Drossart, F. Forget, and T. Fouchet (2007), Hyperspectral imaging of convective CO_2 ice clouds in the equatorial mesosphere of Mars, *J. Geophys. Res.*, *112*, E11S90, doi:10.1029/2007JE002944.

Smith, D. E., M. T. Zuber, and G. A. Neumann (2001), Seasonal variations of snow depth on Mars, *Science*, *294*, 2141–2146.

Smith, M. D. (2009), THEMIS observations of Mars aerosol optical depth from 2002–2008, *Icarus*, *202*, 444–452.

Tillman, J. E., N. C. Johnson, P. Guttorp, and D. B. Percival (1993), The Martian annual atmospheric pressure cycle: Years without great dust storms, *J. Geophys. Res.*, *98*, 10963–10971.

Wilson, R. J., D. Banfield, B. J. Conrath, and M. D. Smith (2002), Traveling waves in the Northern Hemisphere of Mars, *Geophys. Res. Lett.*, *29*, 1684, doi:10.1029/2002GL014866.

Yamashita, Y., T. Kuroda, and M. Takahashi (2007), Maintenance of zonal wind variability associated with the annular mode on Mars, *Geophys. Res. Lett.*, *34*, L16819, doi:10.1029/2007GL030069.